Vector beams generated with a Fourier transform processor with geometric phase grating

Jeffrey A. Davis,[a] Ignacio Moreno,[b,c,*] María del Mar Sánchez-López,[b,d] and Don M. Cottrell[a]

[a]San Diego State University, Department of Physics, San Diego, California, United States
[b]Universidad Miguel Hernández de Elche, Instituto de Bioingeniería, Elche, Spain
[c]Universidad Miguel Hernández de Elche, Departamento de Ciencia de Materiales, Óptica y Tecnología Electrónica, Elche, Spain
[d]Universidad Miguel Hernández de Elche, Departamento de Física Aplicada, Elche, Spain

Abstract. In this work, we present a method to generate vector beams with a 4f polarization Fourier filtering system that combines a spatial light modulator (SLM) at the input plane and a polarization diffraction grating (PDG) at the output plane. In the Fourier plane, two quarter-wave plates are employed to transform the $+1$ and -1 diffraction orders onto circular right (RCP) and left (LCP) polarizations, respectively. The PDG at the output plane recombines the two beams producing the colinear superposition of RCP and LCP beams. The application of a random encoding technique to multiplex diffractive elements on the SLM allows the independent encoding of different patterns on the final beam, thus arbitrary vector beams can be generated at the output. Experimental results are included that demonstrate the capability for this approach to encode a variety of polarization vector beams with different topological charges. [DOI: 10.1117/1.OE.62.1.013104]

Keywords: vector beams; spatial light modulators; polarization diffraction grating; optical processing.

Paper 20221095G received Sep. 23, 2022; accepted for publication Jan. 9, 2023; published online Jan. 28, 2023.

1 Introduction

Vector beams have attracted much attention in the last years, and a variety of methods for their generation have been devised.[1] The most successful techniques employ patterned linear retarders known as q-plates[2] or use spatial light modulator (SLM) programmable devices.[3] In both cases, the effective generation of pure vector beams implies the collinear superposition of a circular right (RCP) and a left (LCP) polarization light vortex beam, each carrying azimuthal phases with opposite topological charge $\ell_R = -\ell_L$. For arbitrary values of the charges, the so-called hybrid vector beams are generated.[4,5]

Here we concentrate on an earlier approach to generate vector beams, which is based on a classical Fourier transform 4f processor.[6–8] This system employs a diffraction grating to split the incoming beam, using a polarization filter at the Fourier plane that uses two discrete quarter-wave plates (QWPs) to filter the ± 1 diffraction orders and transform their polarization states. Finally, another diffraction grating is used at the output plane to recombine the output vector beam.

In the last years, there has also been a great advance in the development of new polarization sensitive diffractive components based on the geometric phase (also named as Pancharatnam-Berry phase).[9] These are typically half-wave plate (HWP) retarders where the principal axis follows a spatial variation. They can be fabricated with liquid-crystal materials[10] or with metamaterials.[11] Geometric phase polarization diffraction gratings (PDG) are commercially available nowadays.

*Address all correspondence to Ignacio Moreno, i.moreno@umh.es

One interesting aspect of these PDG is that they directly produce two diffraction orders with circular polarization, i.e., they act as a circular polarization diffractive beam-splitter. Thus, their use in the 4f Fourier processor directly enables manipulating the output vector beam in terms of the RCP and LCP components, which is the natural decomposition for vector beams.

Therefore, here we propose and experimentally demonstrate a Fourier transform 4f processor with polarization transformation in the Fourier plane for the generation of arbitrary vector beams. Our system follows previous similar systems,[6] but we introduce four significant differences in the system: (1) we use two blazed phase diffraction gratings displayed onto a first SLM located at the input plane to efficiently generate two diffraction orders in the Fourier plane; (2) we apply a random-pattern based multiplexing technique to combine these two blazed gratings and encode additional arbitrary spiral phases onto each diffraction order; and (3) the transformation of the polarization of the two beams in the Fourier plane into circularly polarized light is performed with a second liquid crystal SLM instead of the two discrete QWPs. This approach allows a more precise alignment of the QWPs and allows them to be placed closer together. Finally, (4) we use a PDG in the output plane to efficiently recombine the two beams and produce the output vector beam. All these advances provide the system with a great flexibility and efficiency.

As it will be shown, the system requires precise relations between the focal lengths of the lenses and the periods of the diffraction gratings. The PDG at the output plane has a fixed period, and the lenses have fixed focal lengths. However, the period of the blazed gratings that are displayed on the first SLM can be varied so that the two output beams can be sent to the final PDG at the correct angles. This will be discussed further in Sec. 3.

The paper is organized as follows. After this introduction, Sec. 2 introduces the 4f polarization processor and gives details about the experimental system. Section 3 develops a ray matrix analysis of the optical system that allows determining the relations between the required focal length of the lenses and the periods of the diffraction gratings. Section 4 shows experimental results on the effective generation of vector beams, including pure hybrid vector beams. Finally, in Sec. 5, the conclusions of the work are presented.

2 Experimental System and Methods

2.1 *4f Polarization Processor*

Figure 1 shows a scheme of the 4f polarization processor, with a similar approach as used in Ref. 6. A He-Ne laser is first spatially filtered and collimated. The beam is polarized with a linear polarizer (Pol1) whose transmission axis is oriented parallel to the director of a parallel-aligned liquid-crystal SLM, so the beam can be fully phase modulated. Because the SLM is in the input plane (P1) of a 4f Fourier transform processor, the diffraction orders appear focused on the Fourier plane (P2) located at the back focal plane of the first lens (L1). The SLM encodes two modulated blazed diffraction gratings that generate the $+1$ and -1 diffraction orders in the Fourier plane, as described later.

The Fourier filter includes elements to change the polarization states of these ± 1 diffraction orders, which are yet to be linearly polarized. Following Ref. 6, two QWPs (QWP1 and QWP2) are usually placed on each diffraction order to transform them into circularly polarized light. If QWP1 is oriented with $+45$ deg with respect to the input polarization while QWP2 is oriented with -45 deg, the diffraction orders are transformed into RCP and LCP light beams.

Instead in this work, we use another parallel-aligned SLM onto which the two QWPs can be encoded. We use a HWP to rotate the incident beam at 45 deg. Then we can encode the required phases onto each part. This has a significant advantage. The two QWPs can be placed much closer to each other than is usually possible with discrete elements. In addition, other possible diffraction orders in the Fourier plane are filtered, including the zero-order that might appear on-axis caused either by the modulation characteristics of the SLM or by the encoding technique.

The second part of the 4f system performs a second Fourier transform. Now the two beams are collimated but intersect the output plane (P3) at opposite angles. A diffraction grating placed at this output plane recombines the two beams on axis and makes them collinear, thus creating

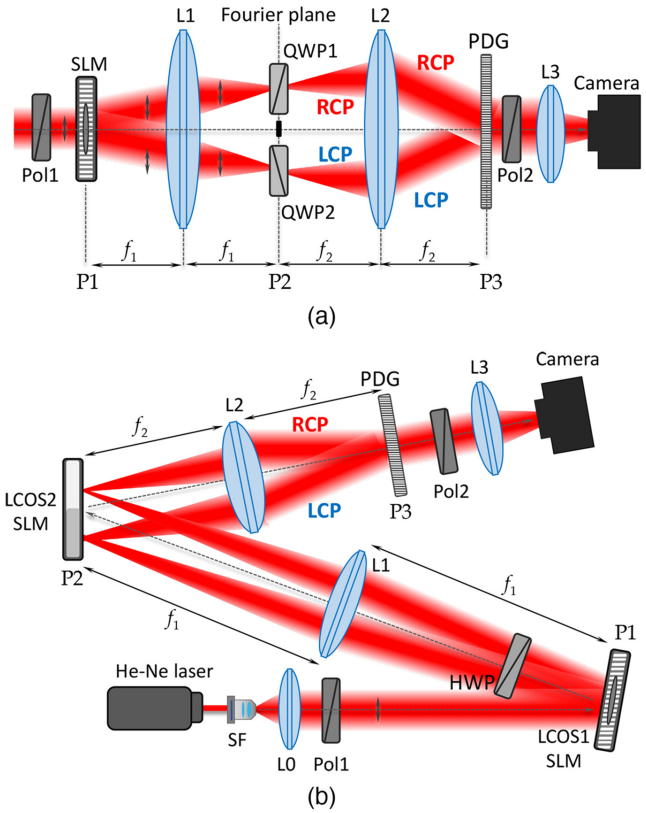

Fig. 1 (a) Scheme of the experimental 4f polarization processor setup. (b) Practical implementation with LCOS-SLMs. L, converging lens; SF, spatial filter; Pol, linear polarizer; SLM, spatial light modulator; HWP, half-wave plate; QWP, quarter-wave plate; and PDG, polarization diffraction grating. P1, input plane; P2, Fourier plane; and P3, output plane.

a common-path diffractive interferometer.[6] In this work, we use a geometric-phase PDG to perform this function. Finally, the output is analyzed by inserting a second polarizer (Pol2) before the camera detector. A lens (L3) is added behind the output plane to change the focus of the output beam.

In practice, we employ liquid-crystal on silicon (LCOS) SLM devices. This is the most common SLM technology nowadays.[12] Because these are reflective devices, the system must be adapted to a reflective geometry as shown in Fig. 1(b). The LCOS-SLM lying in the input plane is an Exulus-HD1/M from Thorlabs with 1920×1080 pixels, with 6.4 μm pixel pitch and parallel-aligned liquid-crystal configuration.

The Fourier transform is formed at the intermediate plane (P2) by means of a lens L1 with 75 cm focal length. In the Fourier plane, instead of using two different QWPs as in Fig. 1(a), we place a second parallel-aligned LCOS device from Santec, model SLM100 with 1440×1050 pixels and 10.0×10.4 μm pixel pitch. This second SLM panel (LCOS2) is divided in two halves and the retardance is adjusted in each side to provide $\pi/2$ and $3\pi/2$ phase shifts, thus acting as a QWP and as a three-QWP, respectively. Therefore, for incident linear polarization oriented at 45 deg with respect to the LCOS2 director axis, each side transforms the polarization into RCP and LCP states, respectively. A HWP is placed after the first SLM to properly orient the linear polarization incident on the second SLM.

Finally, the second Fourier transform is produced with lens L2 and the PDG recombines the two beams to form the output vector beam. Note that we use a lens with a different focal length f_2. Consequently, the periods of the input and output diffraction gratings must be precisely adjusted to the focal lengths of lenses L1 and L2, as described in Sec. 3, to achieve the correct recombination leading to a single output beam. But first, let us next explain the encoding technique used to generate the input modulated phase diffraction grating displayed on LCOS1-SLM.

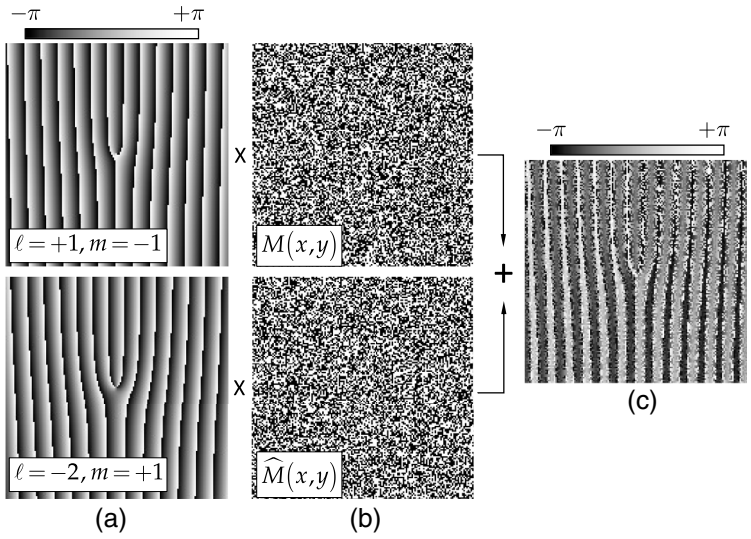

Fig. 2 Example of the phase mask design: (a) fork gratings, (b) binary amplitude random masks, and (c) multiplexed phase-only function.

2.2 *Encoding the Multiplexed Diffraction Grating*

Figure 2 shows an example of the design of the diffraction grating addressed to the input SLM. Since an independent control of the topological charge encoded onto the $+1$ and -1 diffraction orders is desired, we first design two different fork gratings [Fig. 2(a)]. These fork gratings are the result of combining a linear phase and a spiral phase.[13] The example in Fig. 2(a), first row, shows a first fork grating where the linear phase grows from right to left, thus generating the diffraction order with index $m = -1$, and with an encoded spiral phase of charge $\ell = -1$. On the other hand, the fork grating in the second row has a spiral phase with $\ell = +2$ and the linear phase grows from left to right, thus generating the positive diffraction order $m = +1$.

The combination of these two gratings is achieved using the random multiplexing technique.[14,15] A random binary mask $M(x, y)$ is generated, where each pixel randomly takes values 1 and 0 [white and black pixels in Fig. 2(b)]. This binary function multiplies the first fork grating, whereas the complementary binary function $\hat{M}(x, y) = 1 - M(x, y)$ multiplies the second fork grating. The two resulting functions are added to produce the multiplexed phase-only function in Fig. 2(c). This phase function, when displayed on the phase-only LCOS1-SLM basically generates the two diffraction orders, each one with the corresponding encoded spiral phase. This encoding technique allows therefore an independent topological charge encoded on each order, as opposed to the method used in Ref. 6. We also note that displaying the gratings on the SLM allows a very precise selection of their period, which is crucial for adjusting the system as explained in Sec. 3.

2.3 *Beam Recombination with a Geometric-Phase Polarization Diffraction Grating*

Another interesting variation with respect to Ref. 6 is that here we use a geometric-phase PDG at the output plane to produce the collinear combination of the RCP and LCP beams that generates the output vector beam. Figures 3(a) and 3(b) illustrates the peculiar effect of such PDG gratings. When illuminated with RCP light with normal incidence, the input beam is fully transformed onto LCP and fully diffracted by an angle $\theta = \lambda/d_{\mathrm{PDG}}$ onto the $+1$ diffraction order.[16] Here d_{PDG} is the grating's period and λ is the wavelength, and the small angle paraxial approximation is considered. On the contrary, LCP input polarization is fully transformed onto RCP and diffracted in the opposite direction onto the -1 diffraction order. The grating thus acts as a diffractive polarization beam splitter. If the input beam is linearly polarized it splits into two equally intense orders.

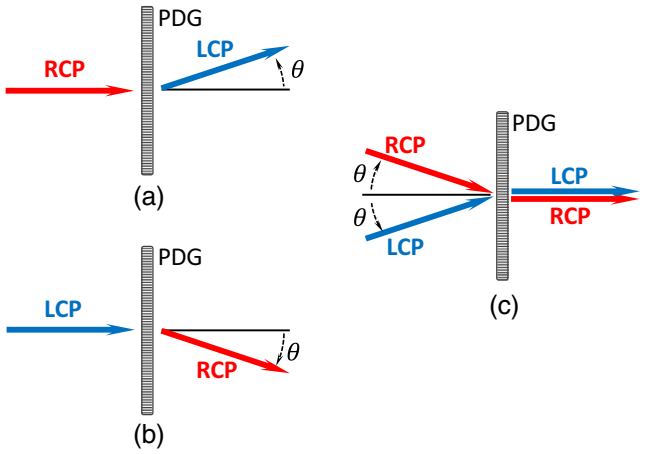

Fig. 3 Principle of operation of the geometric phase PDG.

Figure 3(c) illustrates the behavior of the grating the way it is employed in this work. Here the PDG is illuminated simultaneously with an RCP and an LCP beam of incident angle $+\theta$ and $-\theta$, respectively. In this situation, the beams diffract in opposite directions since they have opposite circular polarizations, and the output is the on-axis collinear superposition of the two beams. This configuration thus represents a very efficient and direct way of recombining the output of a 4f polarization processor to obtain the output vector beam since no other diffraction orders are generated apart from the one of interest.

However, before presenting experimental results, some discussion of the correct matching between the gratings' periods and lenses focal lengths is required. This is discussed in the next section.

3 Ray Matrix Discussion

Simple ray matrix theory[17] provides an insight into the system. In this formalism, light rays are described as

$$\mathbf{r} = \begin{bmatrix} r \\ r' \end{bmatrix}, \tag{1}$$

where r and r' denote the position and angle of the ray. Figure 4 illustrates this calculation for the system in our work. We consider the input plane P1 illuminated with a collimated beam, thus $r_1' = 0$ can be considered in the plane just before P1. In this plane, a blazed diffraction grating having a period of d_1 generates a single diffracted beam where the output angle is now $r_1' = \lambda/d_1$, according to the diffraction grating law. When this beam is focused on plane P2

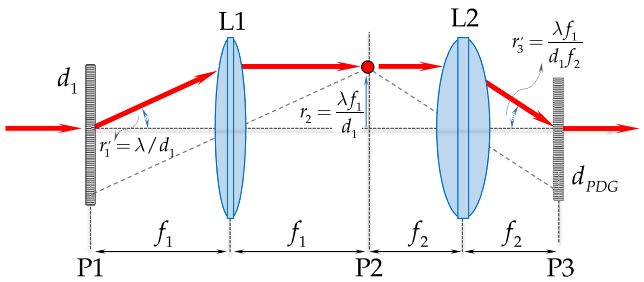

Fig. 4 Illustration to derive the gratings' period to lenses focal lengths relation. d_1 and d_{PDG} denote the period of the diffraction gratings at planes P1 and P3, respectively.

by the lens L1 having focal length f_1, the position of the Fourier transform plane P2 is given as

$$r_2 = \frac{\lambda f_1}{d_1}. \tag{2}$$

Now, after the second Fourier transform produced with lens L2, the corresponding ray impinging on plane P3 arrives with an angle given as

$$r_3' = -\frac{r_2}{f_2} = -\frac{\lambda f_1}{d_1 f_2}, \tag{3}$$

where the minus sign accounts for the change of orientation of the output ray compared to the input one.

However, this angle must exactly match the diffraction angle for the PDG to have the output collimated along the optical axis. This angle is related to the PDG period d_{PDG}, namely $r_3' = \lambda/d_{\mathrm{PDG}}$. Consequently, the experimental system requires that the following equality must be satisfied

$$\frac{f_1}{f_2} = \frac{d_1}{d_{\mathrm{PDG}}}, \tag{4}$$

i.e., the ratio of focal lengths must be the same as the ratio of the gratings' period.

In our final setup, we used the PDG model PG-5 manufactured by ImagineOptix having an angle of 5 deg for each beam relative to the optical axis, which corresponds to $d_{\mathrm{PDG}} \approx 7\,\mu$m. Note that a large value of d_1 is convenient because it reduces the impact of quantization errors in the input grating. However, if d_1 is large, the separation between the ± 1 diffraction orders in the Fourier plane is small, which makes it difficult their polarization filtering. This can be compensated with a large focal length f_1. In our final system we used lenses with focal lengths of $f_1 = 75$ cm and a photographic objective lens with $f_2 = 5$ cm.

Because the LCOS1-SLM is employed to display the input grating, we were able to accurately tune the gratings' period in order to satisfy Eq. (4). We used input phase gratings with periods of 17 pixels in SLM1 (i.e., $d_1 \approx 108\,\mu$m). This number of pixels per period ensures that the efficiency is not affected by quantization.[18] Nevertheless, the random masks multiplexing technique described in Sec. 2.2 reduces the efficiency and some DC term is present, which must be filtered in the Fourier plane.

We note that with these values, the Fourier planes are separated by a total distance of about 0.6 mm. Therefore, it would be difficult to use two discrete QWPs to change the polarizations of these two beams. Using a second properly oriented LCOS in the Fourier plane, we can encode the two QWPs more accurately than would be possible using discrete elements.

4 Experimental Results and Discussion

Figure 5 shows a first set of experiments where we illustrate the alignment of the system. Here a vector beam is built by encoding charges $\ell_R = -2$ and $\ell_L = +2$ on the RCP and LCP beams, respectively. The lens L3 on the system is adjusted to provide on the camera an image of the output plane (which is also image of the input plane). In the captures on the left [Figs. 5(a) and 5(e)], the two beams appear clearly separated because the grating's period in LCOS1-SLM does not match the period of the PDG (Eq. (4) is not fulfilled). Some interference fringes appear only in the central region of superposition of the two beams.

The condition in Eq. (4) can be approached by tuning the period d_1 of the input grating and the two beams feature a larger overlap region and the fringes become wider. The presence of the singularity is clear, and the interference pattern adopts a fork shape[19] [Figs. 5(b) and 5(f)]. When the good alignment is almost reached, the interference pattern shows only four lobes, but they show a deformation [Figs. 5(c) and 5(g)]. Finally, when the alignment is reached the four-lobe pattern characteristic of the vector beam with charge 2 is obtained [Fig. 5(d)].

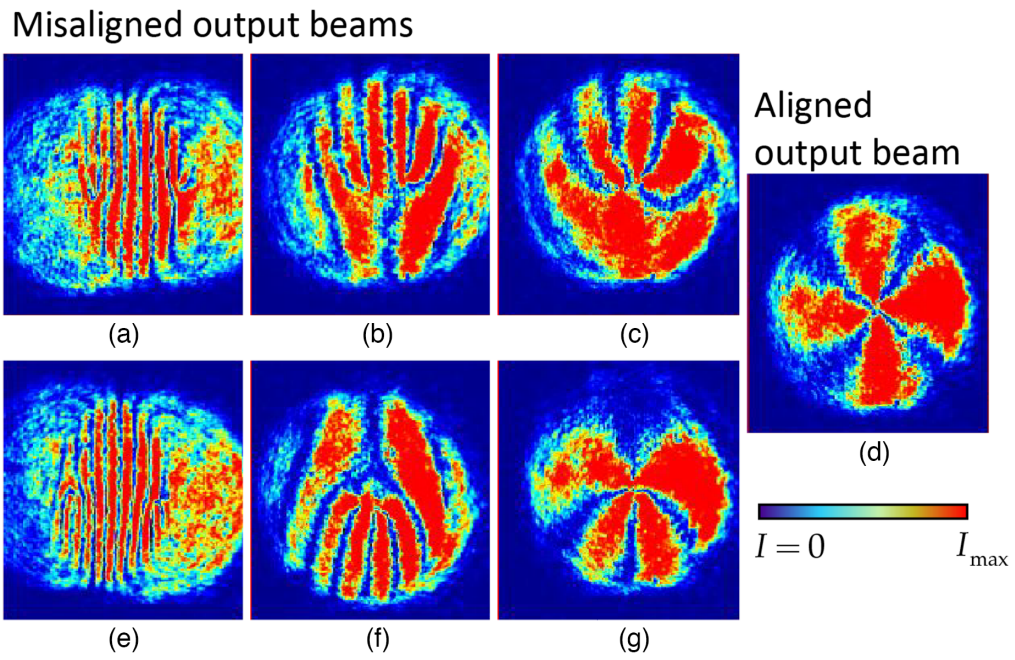

Fig. 5 Experimental demonstration of the alignment of the output vector beam.

As Fig. 5 shows, the direction of the fork type fringes changes its sense when the mismatch between the periods d_1 and d_{PDG} is in excess or in defect with respect to Eq. (4). Finally, let us remark that a similar behavior was observed when there is a rotation between the input grating on LCOS1-SLM and the output PDG.

Next, we changed the position of lens L3 to focus the output vector beam. Figure 6 shows a first set of experimental results, where the successful generation of pure vector beams is demonstrated. Here, topological charges with opposite sign $\ell_L = -\ell_R = 1, 2, 3, 5, 10$ were encoded on the ± 1 diffraction orders. When the intensity distribution is captured, with no analyzer in front of the camera, the output presents the classical doughnut shaped beam where the phase singularity on the center of the beam results in a dark region with larger diameter as the topological charge increases. The results in Fig. 6 also show the captures when a linear polarizer is used as an analyzer, with horizontal, vertical, and ± 45 deg orientations. The effective generation of the vector beams is proven by the formation of petal beam patterns,[20] i.e., annular beams showing $|\ell_R - \ell_L|$ azimuthal lobes. Note that there is indeed an even number of lobes, which rotate as we rotate the analyzer.

A second set of experiments demonstrating the possibility of generating hybrid vector beams is shown in Fig. 7. Here, different topological charges are encoded on each diffraction order. We consider $(-1, +2)$ and $(-2, +3)$, so there is little difference in the diameter of the doughnut. In this situation, the successful generation of the hybrid vector beam is shown by the odd number of azimuthal lobes, given by $|\ell_R - \ell_L|$.

Finally, Fig. 8 shows examples of vector beams with $\ell_R = -\ell_L = 3$ where the ratio between the RCP and LCP components is not equally weighted as opposed to the previous cases. In this situation, the resulting vector beam no longer has linear polarization states. Instead, it is formed by elliptical states that rotate azimuthally. We achieve this simply by changing the number of white and black pixels assigned to the binary mask $M(x, y)$ in Fig. 2.

The previous results in Figs. 6 and 7 were obtained with a ratio $R = 50\%$, so both diffraction orders had the same intensity. Here in Fig. 8 we change the ratio to $R = 55\%$, $R = 65\%$, $R = 85\%$, and finally $R = 100\%$ (in this last case, only one diffraction order is produced). The effect is a progressive reduction of the contrast between the azimuthal lobes. Because the states in the vector beam are azimuthally rotating elliptical states, there is never a cancellation when rotating the analyzer. In the limiting case with $R = 100\%$, there is only one circular polarization component in the output beam, and this is just a vortex beam. The fact that for all positions

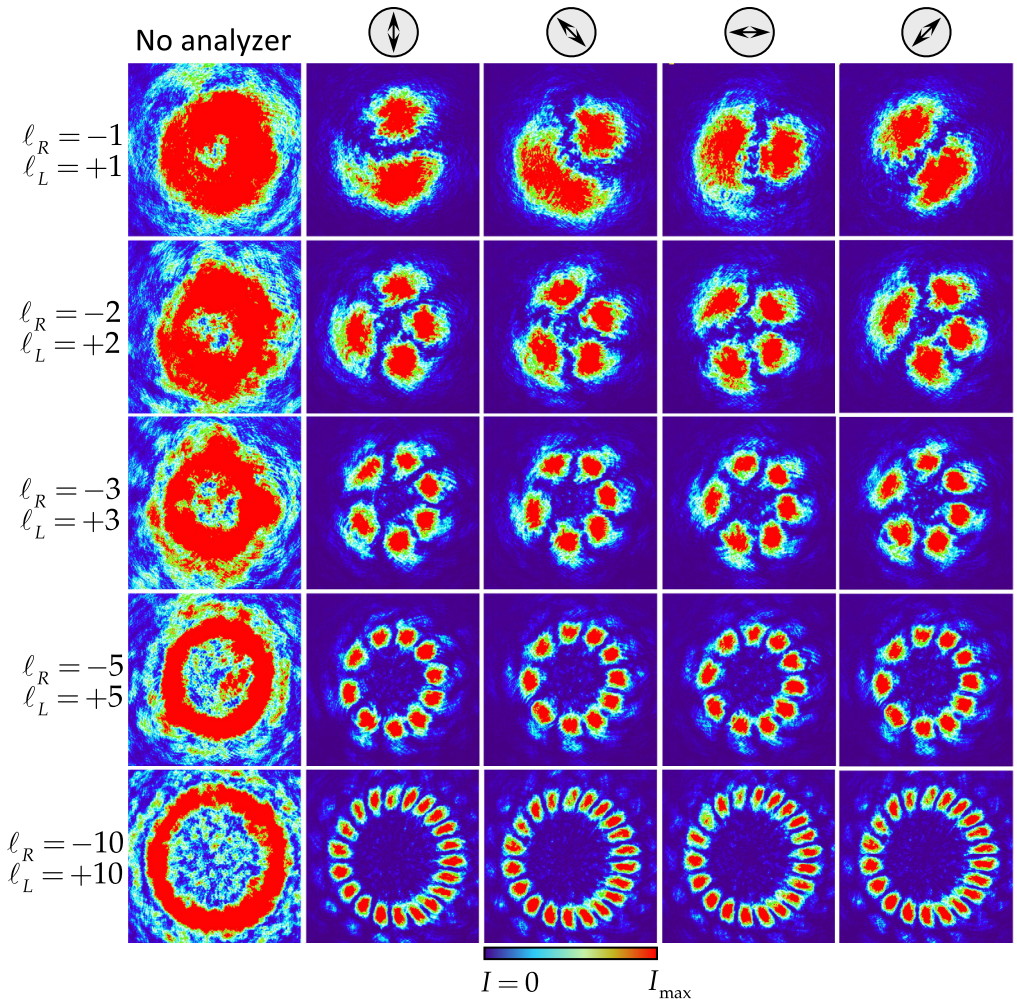

Fig. 6 Experimental generation of pure vector beams with different topological charge.

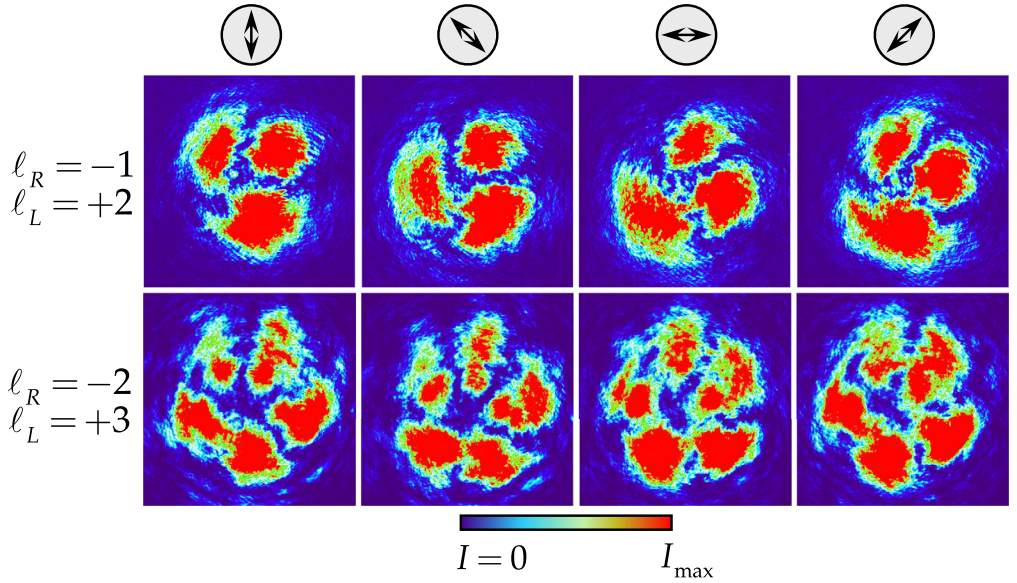

Fig. 7 Experimental generation of hybrid vector beams with different topological charge.

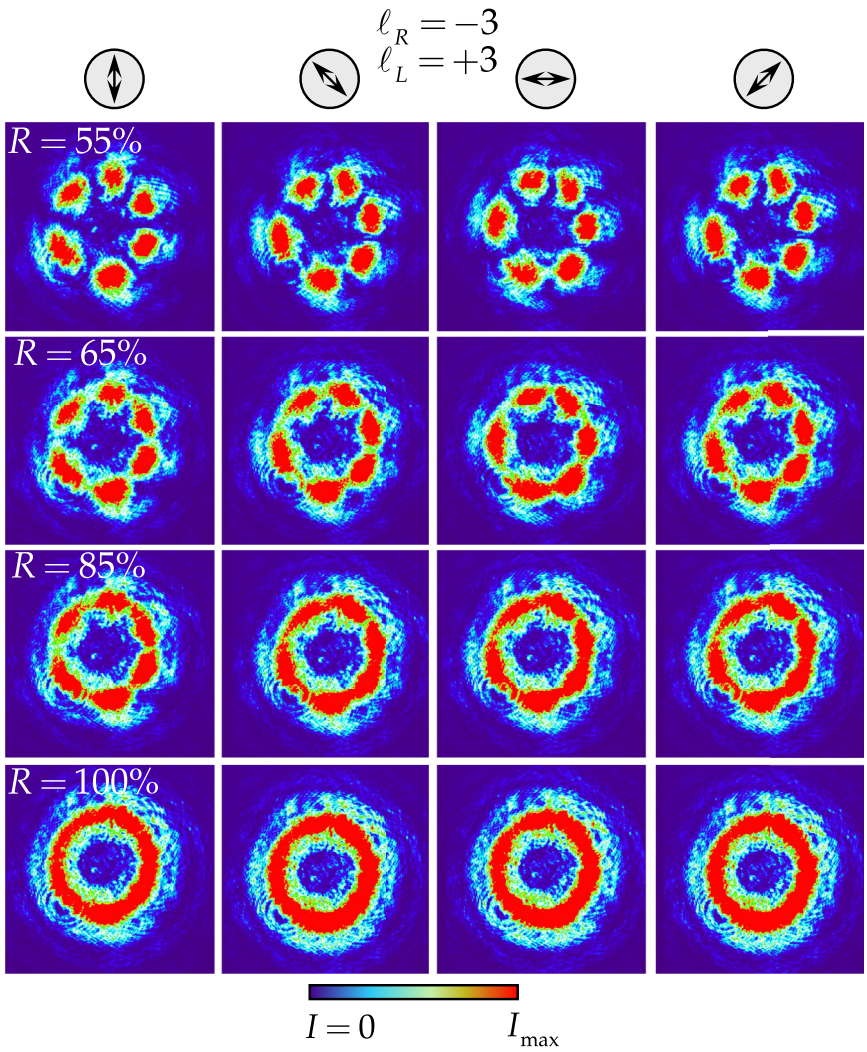

Fig. 8 Experimental generation of vector beams with topological charge $\ell = 3$ and different ratios of RCP and LCP components. R denotes the percentage of pixels in the mask diffracting to the $+1$ diffraction order.

of the analyzer we obtain the complete circle of light, with no azimuthal variation, denotes that the beam is circularly polarized.

5 Conclusions

In summary, we proposed and experimentally demonstrated a Fourier transform 4f processor with polarization transformation in the Fourier plane that enables the generation of vector beams. Our system follows previous similar systems,[6] but we introduce four significant differences that adds great flexibility and efficiency to the system: (1) we use two blazed phase diffraction gratings at the input plane to efficiently generate two diffraction orders in the Fourier plane; (2) we apply a random-pattern based multiplexing technique to combine these two blazed gratings and encode additional arbitrary spiral phases onto each diffraction order; (3) the transformation of the state of polarization in the Fourier plane is performed with a second LCOS-SLM, rather than two discrete QWPs, which allows a precise and fine adjustment of their positions; and finally, (4) we use a PDG in the output plane to efficiently recombine the two beams and produce the output vector beam.

We presented an analysis based on the ray matrix approach that provides the required relations to accurately adjust the diffraction gratings' periods, relative to the focal lengths of the

two lenses in the system. The experimental results presented show the successful generation of output vector beams. We believe these results show an example of the great potential that PDG and other geometric phase diffractive elements might achieve in the design of efficient optical systems for polarization control.

Acknowledgements

IM and MMSL acknowledge financial support from Ministerio de Ciencia e Innovación, Spain (Grant No. PID2021-126509OB-C22) and Conselleria d'Innovació, Universitats, Ciència i Societat Digital, Generalitat Valenciana (Grant No. CIAICO/2021/276). The authors declare no conflicts of interest.

References

1. S. Pachava et al., "Generation and decomposition of scalar and vector modes carrying orbital angular momentum: a review," *Opt. Eng.* **59**(4), 041205 (2019).
2. A. Rubano et al., "Q-plate technology: a progress review," *J. Opt. Soc. Am. B* **36**, D70–D87 (2019).
3. C. Rosales-Guzmán, B. Ndagano, and A. Forbes, "A review of complex vector light fields and their applications," *J. Opt.* **20**, 123001 (2018).
4. S. Lou et al., "Generation of arbitrary vector vortex beams on hybrid-order Poincaré sphere based on liquid crystal device," *Opt. Express* **27**(6), 8596–8604 (2019).
5. J. C. Quiceno-Moreno et al., "Analysis of hybrid vector beams generated with a detuned q-plate," *Appl. Sci.* **10**, 3427 (2020).
6. X.-L. Wang et al., "Generation of arbitrary vector beams with a spatial light modulator and a common path interferometric arrangement," *Opt. Lett.* **32**(24), 3549–3551 (2007).
7. H. Chen et al., "Generation of vector beam with space-variant distribution of both polarization and phase," *Opt. Lett.* **36**(16), 3179–3181 (2011).
8. I. Moreno et al., "Jones matrix treatment for optical Fourier processors with structured polarization," *Opt. Express* **19**(5), 4583–4594 (2011).
9. N. A. Rubin, Z. Shi, and F. Capasso, "Polarization in diffractive optics and metasurfaces," *Adv. Opt. Photonics* **13**(4), 836–970 (2021).
10. J. Kim et al., "Fabrication of ideal geometric-phase holograms with arbitrary wavefronts," *Optica* **2**(11), 958–964 (2015).
11. R. Drevinskas and P. G. Kazansky, "High-performance geometric phase elements in silica glass," *APL Photonics* **2**, 066104 (2017).
12. Z. Zhang, Z. You, and D. Chu, "Fundamentals of phase-only liquid crystal on silicon (LCOS) devices," *Light: Sci. Appl.* **3**, e213 (2014).
13. V. Y. Bazhenov, M. V. Vasnetsov, and M. S. Soskin, "Laser beams with screw dislocations in their wavefronts," *J. Mod. Opt.* **39**(5), 985–990 (1990).
14. J. A. Davis et al., "Multiplexed phase-encoded lenses written on spatial light modulators," *Opt. Lett.* **14**(9), 420–422 (1989).
15. J. A. Davis and D. M. Cottrell, "Random mask encoding of multiplexed phase-only and binary phase-only filters," *Opt. Lett.* **19**(7), 496–498 (1994).
16. B. Gao, J. Beeckman, and K. Neyts, "Design and realization of a compact efficient beam combiner based on liquid crystal Pancharatnam–Berry phase gratings," *Crystals* **11**, 220 (2021).
17. J. A. Davis and R. A. Lilly, "Ray-matrix approach for diffractive optics," *Appl. Opt.* **32**(2), 155–158 (1993).
18. I. Moreno et al., "Diffraction efficiency of stepped gratings using high phase-modulation spatial light modulator," *Opt. Lasers Eng.* **126**, 105910 (2020).
19. I. Moreno et al., "Encoding high order cylindrically polarized light beams," *Appl. Opt.* **53**(24), 5493–5501 (2014).
20. I. A. Litvin, L. Burger, and A. Forbes, "Angular self-reconstruction of petal-like beams," *Opt. Lett.* **38**(17), 3363–3365 (2013).

Jeffrey A. Davis received his BS degree in physics from Rensselaer Polytechnic Institute and his PhD from Cornell University. He is a professor of physics at San Diego State University, where he leads the electro-optics program. His research interests include optical pattern recognition, spatial light modulators, and programmable diffractive optical elements. He is coauthor of more than 200 publications in peer-reviewed journals. He is a fellow of SPIE and of Optica (formerly OSA).

Ignacio Moreno graduated in physics and got his PhD at Autonomous University of Barcelona (UAB). He is professor of optics at University Miguel Hernández (UMH). After two years at University of Valencia, he joined UMH. His research is centered in the field of spatial light modulators for diffractive and polarization optics. He is fellow of SPIE and Optica. He was a president of SEDOPTICA (2017–2020) and he is now member of the board of directors of the European Optical Society (EOS).

María del Mar Sánchez-López graduated in physics and got her PhD both at UAB. She is professor of applied physics at UMH. After a post-doc with INFM, Salerno (Italy), she joined UMH. Her research activity is currently centered on structured light and liquid-crystal-based reconfigurable systems. She is a senior member of SPIE and participated in the 2014–2015 SPIE Women in Optics planner. She is a member of Real Sociedad Española de Física, where she served as a president of its Local Section of Alicante (2017–2021).

Don M. Cottrell received his BS and PhD degrees from the University of Washington. He is an emeritus professor of physics at San Diego State University. His research interests include the computer construction of synthetic holograms and the computer program used in this research. He also conducts theoretical studies in general relativity and particle physics involving differential geometry and supersymmetry.